21. A PERSISTENT JAPANESE HEAT WAVE IN EARLY AUGUST 2015: ROLES OF NATURAL VARIABILITY AND HUMAN-INDUCED WARMING

The persistent Japanese heat wave that occurred in early August 2015 was mainly attributed to intraseasonal disturbances including tropical cyclones. Anthropogenic warming contributed to an increase in the probability of occurrence.

Chiharu Takahashi, Masahiro Watanabe, Hideo Shiogama, Yukiko Imada, and Masato Mori

Introduction. A prolonged heat wave hit Japan in early August 2015. Daily maximum surface air temperature (SAT) exceeded 35°C for eight consecutive days and the 8-day mean anomaly was greater than 4°C at several observation sites, causing over 10 000 people to suffer from heatstroke. This heat wave was particularly unusual because an ongoing extreme El Niño of 2015 was expected to lead to a cooler summer in Japan.

A primary cause of this heat wave was an intraseasonal tropical disturbance (Fig. 21.1). A tropical cyclone (TC), TC1513, was generated in the western North Pacific (WNP) during the convectively active phase of the intraseasonal oscillation (ISO) in the western Pacific (Fig. 21.1c and Supplemental Fig. S21.3c), followed by another TC (TC1514). Li and Zhou (2013) demonstrated that the two major components of the ISO, the 30–60 day Madden–Julian oscillation (MJO, Madden and Julian 1971) and the 10–20 day quasi-biweekly oscillation (QBWO, Chen and Sui 2010) can affect the genesis and intensity of TCs in the WNP during the summer. It appears that the TCs in this study likewise formed in association with the ISO.

The diabatic heating associated with the TC-related precipitation induced a Rossby wave train, which is characterized by cyclonic circulation and anticyclonic circulation anomalies in the WNP and East Asia, respectively (Figs. 21.1b,d). This pattern is similar to the so-called Pacific–Japan (PJ) teleconnection pattern (Nitta 1987; Wakabayashi and Kawamura 2004) in July and August, accompanying a meridional tripolar pattern in precipitation, vorticity, and temperature anomalies (Supplemental Fig. S21.1a). Several studies have also reported that TCs can generate the PJ pattern over the WNP (Kawamura and Ogasawara 2006; Yamada and Kawamura 2007). In early August 2015, the positive PJ pattern gave rise to the abnormally persistent hot and dry days over Japan.

The El Niño conditions climatologically had a cooling impact on Japan in July–August (Supplemental Fig. S21.1a), yet the 2015 summer was still unexpectedly hot (Supplemental Fig. S21.1b). Anthropogenic warming can change the likelihood of specific extreme events, although the odds of an event occurring may vary from year to year depending on the regional sea surface temperature (SST) pattern (Christidis and Stott 2014). In this study, we investigate the possible influences of the intraseasonal variability, the 2015 strong El Niño, and anthropogenic warming on the Japanese heat wave in August 2015 using an atmospheric general circulation model (AGCM).

Methods. We performed four 100-member ensemble experiments using the Model for Interdisciplinary Research on Climate, version 5 (MIROC5), AGCM with a horizontal resolution of 150 km (Watanabe et al. 2010). Each of the four experiments used different initial conditions during January–October 2015: 1) ALL: Experiments designed to simulate the current observed world, forced by the observed historical SST and sea ice (SIC) derived from the HadISST dataset (Rayner et al. 2003) and historical anthropogenic and natural radiative forcing agents; 2) NAT1: Forced by natural forcing agents and historical SST and SIC

AFFILIATIONS: Takahashi and Watanabe—Atmosphere and Ocean Research Institute, University of Tokyo, Chiba, Japan; Shiogama—Center for Global Environmental Research, National Institute for Environmental Studies, Tsukuba, Japan; Imada—Meteorological Research Institute, Tsukuba, Japan; Mori—Research Center for Advanced Science and Technology, University of Tokyo, Tokyo, Japan

DOI:10.1175/BAMS-D-16-0157.1

A supplement to this article is available online (10.1175/BAMS-D-16-0157.2)

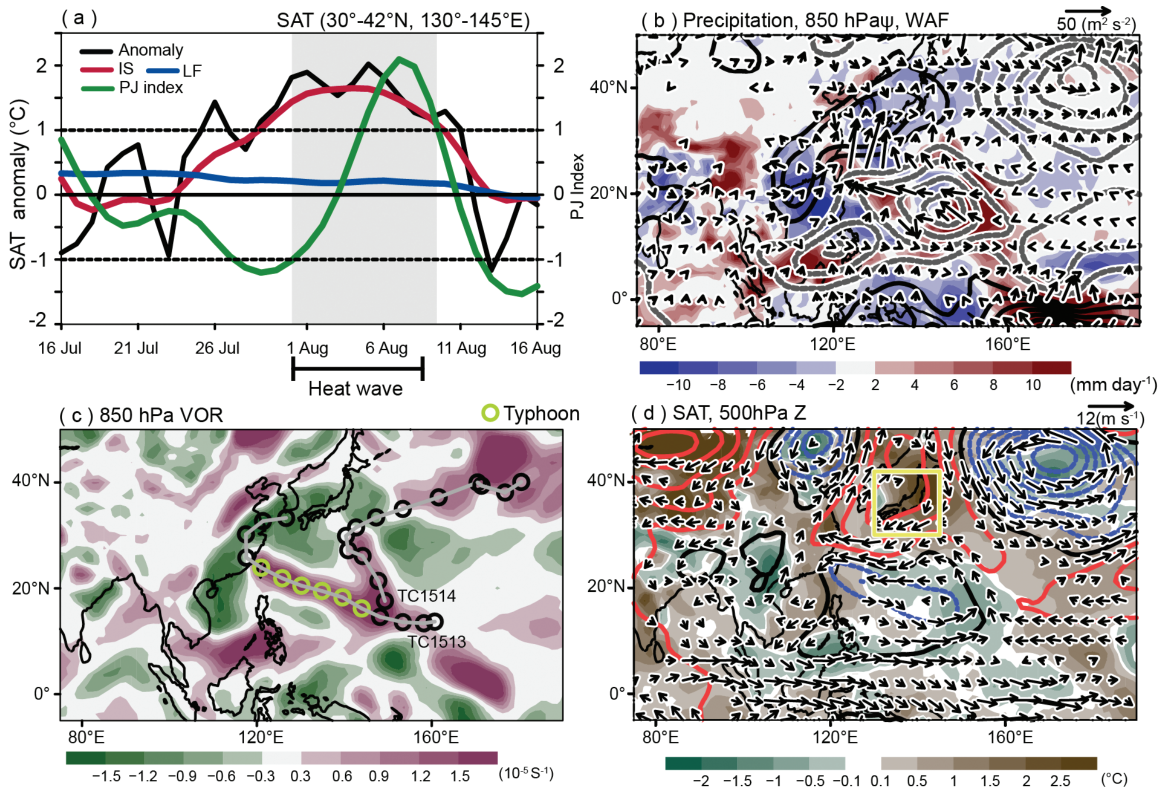

Fig. 21.1. (a) Time series of observed SAT anomalies over Japan (30°–42°N, 130°–145°E, land area only, daily anomaly in black, IS in red, and LF in blue) and normalized PJ index in green from 16 July to 16 Aug 2015. The shading indicates the analysis period (10-day from 31 Jul to 9 Aug) including the heat wave event. (b)–(d) Observed patterns of the 10-day mean anomalies in (b) precipitation (shading), 850-hPa stream function (contours, 10^6 m^2 s^{-1} interval), and 850-hPa wave activity fluxes (vectors); (c) 850-hPa vorticity, on which 2 TC tracks (green and black circles) are superimposed; and (d) SAT (shading), 500-hPa geopotential height (contours, 10-m interval), and 500-hPa winds (vectors). The dashed contours indicate negative anomalies.

excluding anthropogenic forcings by subtracting the long-term 1870–2012 linear trends in SST from the HadISST dataset (Christidis and Stott 2014); 3) NAT2: Similar to NAT1, but forced by SST/SIC excluding anthropogenic forcings by subtracting SSTs estimated using the Coupled Model Intercomparison Project Phase 5 (CMIP5) attribution experiments (Stone 2013); 4) ALLnoENSO: Same as ALL but the SST anomaly that regressed onto the Niño-3.4 SST anomaly was removed in order to eliminate the influence of the extreme El Niño in 2015. The above experiments except for ALLnoENSO were designed by Shiogama et al. (2013, 2014) and updated from the previous runs (Imada et al. 2014). We also performed a 10-member long-term ALL experiment, called ALL-LNG, for 1949–2014, to define the model climatology and evaluate the simulated interannual variability (Supplemental Fig. S21.2). We use the daily JRA–55 Reanalysis dataset (Onogi et al. 2007; Kobayashi et al. 2015) and Global Precipitation Climate Project (GPCP v1.2; Huffman et al. 2001). The TC data was obtained from the best-track of TC provided by the Tokyo–Typhoon Center, Japan Meteorological Agency.

We analyze daily anomalies of all related variables from the daily climatology for 1981–2010. Bandpass (10–60 day) and low pass (60 day) filters are applied to daily anomaly fields in order to extract the intraseasonal (IS) and low frequency (LF) components of natural variability. The IS component is mainly associated with the PJ pattern that links to TCs, and the LF part is related to seasonal variability including the influence of the 2015 El Niño. The SAT anomaly in Japan was largely dominated by the IS component in mid-July to mid-August (Fig. 21.1a). To examine the variability of the intraseasonal PJ pattern, the empirical orthogonal function (EOF) analysis is performed to intraseasonal 850-hPa vorticity anomalies in the domain of 10°–50°N, 110°–170°E in July and August for 1981–2015 in the observation and for 2015 in the ALL ensemble. The intraseasonal PJ index is defined as the principal component associated with the leading EOF that accounts for 8.3% of the total variance in the observation. The observed intraseasonal PJ index exceeded 1 standard deviation (σ) in the period of the heat wave in 2015 (Fig. 21.1a). We mainly analyze the 10-day period from 31 July to 9 August 2015 to cover the extreme heat event (Fig. 21.1a).

Results. The PJ pattern simulated in the ALL 100-member ensemble corresponds well with the observational pattern (Supplemental Figs. S21.3.a,b). A few ensemble members in ALL had SAT anomalies over Japan equal to or higher than the observation (extreme warm members) and well represent the positive PJ patterns induced by northwestward-propagating TC-like disturbance as in the observations (Supplemental Figs. S21.3d–f). Apart from the PJ pattern originating from TCs, an upper-tropospheric wave train also appears in the observation (Supplemental Fig. S21.3g). Ogasawara and Kawamura (2007) suggest that a combined effect of the PJ pattern and other teleconnection patterns propagating from the west may cause extraordinary summer weather. However, the extreme warm members in the ALL experiment do not exhibit a clear upper-level wave train (Supplemental Fig. S21.3h), suggesting that the PJ pattern played the key role in the occurrence of the 2015 extreme heat.

The simulated SAT anomalies (T) are decomposed into IS (T_{IS}) and LF (T_{LF}) components for the 10-day period that includes the heat wave. The observed total and IS SAT anomalies are 1.7°C and 1.4°C averaged over Japan's land area (30°–42°N, 130°–145°E), respectively, indicating that the IS component mostly explains the total SAT anomaly (Fig. 21.2a). The relative contributions of anthropogenic forcing and El Niño to the 2015 extreme heat wave are evaluated. The occurrence probability of an extreme warm event that exceeds or is equal to the observed SAT anomaly is estimated using the probability density function (PDFs) based on the assumption of a Gaussian distribution in each run. The best estimates (50th percentile) and uncertainties (the 5%–95% range) of the probabilities are estimated through random resampling. The best estimate in occurrence probability (the 5%–95% uncertainty range) of the 2015 extreme event is 2.8% (1.2%–4.7%) for ALL, 1.8% (0.7%–3.4%) for NAT1, 1.6% (0.6%–2.8%) for NAT2, and 4.5% (2.2%–7.0%) for ALLnoENSO (Fig. 21.2c). The results suggest that the anthropogenic warming contributed to increase the probability of the 2015 heat wave by 1.5 to 1.7 times (5%–95% range: 0.6–5.0), while the El Niño condition acted to counteract the anthropogenic warming effect and decrease the probability by 0.6 times (5%–95% range: 0.2–1.5).

We also investigate why the low-frequency SAT in Japan during the 2015 heat wave unexpectedly exhibits positive anomalies (Fig. 21.1a) in spite of the strong El Niño year. The influences of anthropogenic forcing and El Niño on T_{LF} can be estimated from the difference between ALL and NAT (T_{GW1} and T_{GW2}), and ALL and ALLnoENSO (T_{ENSO}), respectively (Fig. 21.2b). The ensemble mean of T_{LF} in ALL is approximately consistent with that in observation (Figs. 21.2a,d). The ensemble mean with 1 σ is 0.60°C ± 0.42°C for T_{GW1}, 0.44°C ± 0.46°C for T_{GW2}, and −0.24°C ± 0.44°C for $T_{ENSO.}$ In observation, the SAT anomaly in Japan is −0.19°C ± 0.31°C for the warm phase of the ENSO, when Niño-3.4 SST anomaly is greater than 0.7 σ in July–August for 1958–2014. These results indicate that the 2015 El Niño (T_{ENSO}) has a cooling impact on temperatures in Japan comparable to that of the climatology for other El Niño years and suggest that the impact of anthropogenic warming overcomes the cooling effect by the El Niño. However, an individual atmospheric response to SST variability in the tropics has large variation for the observation and the simulation. The best estimate (the 5%–95% range) of the probability exceeding the observed anomaly (0.20°C) for T_{LF} by similar resampling is 48.6% (43.0%–54.7%) for ALL, 8.3% (5.3%–12.2%) for NAT1, 18.3% (13.7%–22.8%) for NAT2, and 69.5% (64.7%–74.8%) for ALLnoENSO (Fig. 21.2d). This result also suggests that anthropogenic forcing caused a significant increase in the probability of a seasonally warm 2015 summer in Japan, while the El Niño decreased it.

As LF components are better captured by the ALL ensemble, we focused on the anthropogenic and El Niño contributions to T_{LF} over a wider region. In observations, positive T_{LF} anomalies over Japan are accompanied by anticyclonic circulation anomalies, which may be part of a wave train emanating from the subtropical WNP through the North Pacific to the west coast of North America that appears to be a seasonally generated positive PJ pattern (Fig. 21.2e). The changes in the atmospheric circulation owing to anthropogenic warming and El Niño, represented by T_{GW2} and $T_{ENSO,}$ show a different structure (Figs. 21.2g,h). The change in atmospheric temperature as a result of anthropogenic global warming simulated by climate models shows strong warming over the polar region in the lower- to mid-troposphere (e.g., Simpson et al. 2014). This change indicates that the midlatitude

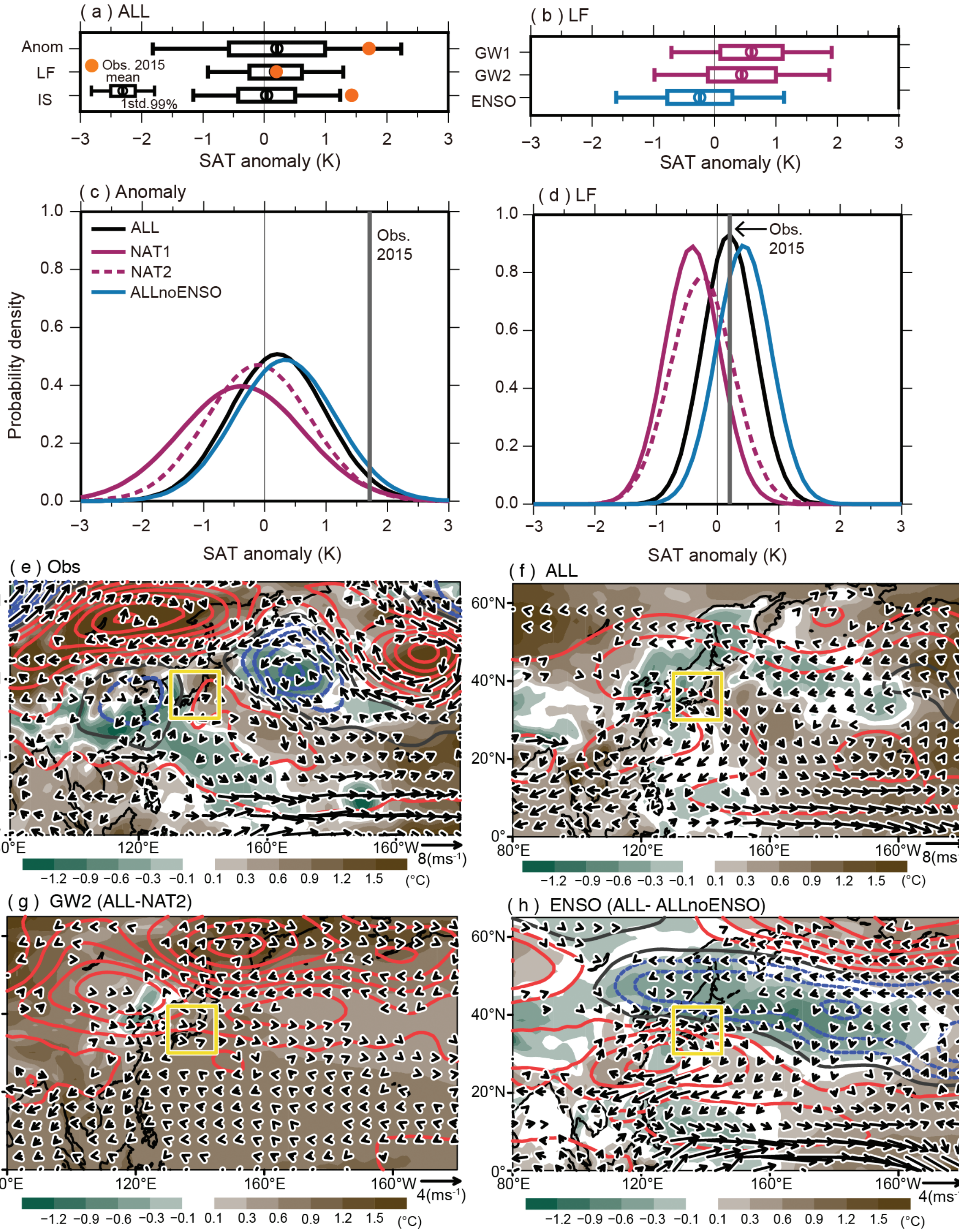

Fig. 21.2. (a) Box-and-whisker plots of 10-day average SAT anomalies over the Japan land area [boxes in (e),(f)] in 2015 event. Daily anomalies, LF, and IS components in ALL are compared with observations (orange circles). (b) As in (a) but contributions of global warming and ENSO to LF in ALL. GW1, GW2, and ENSO represent the differences of SAT anomalies between ALL and NAT1, NAT2, and ALLnoENSO, respectively. (c)–(d) PDFs of the 10-day averaged SAT over Japan for (c) daily anomalies and (d) LF components. (e)–(h) 10-day average LF SAT (shading), 500-hPa geopotential height [contours, 10-m and 3-m intervals with negative dashed in (e),(f) and (g),(h), respectively], and 850-hPa winds (vectors) anomalies for (e) Obs, (f) ALL, (g) GW2, and (h) ENSO. Anomalies in (f)–(h) represent the 100-member ensemble means.

circulation undergoes a poleward shift and thus the equator-to-pole temperature gradient decreases. The change in circulation patterns due to the anthropogenic effect (T_{GW2}) likewise represents the midlatitude anticyclones with SAT and SST warming (Fig. 21.2g). On the other hand, the El Niño-induced teleconnection pattern in 2015 formed a wave train propagating from the tropical western Pacific northward and acts to decrease the seasonal SAT accompanied by the anomalous cyclonic circulation over Japan that links to a suppressed northward expansion of the climatological North Pacific high (Fig. 21.2h). The seasonal PJ pattern in summer tends to have negative correlations with El Niño–Southern Oscillation (ENSO) in the preceding boreal winter and with Indian Ocean temperature in the concurrent summer (Kubota et al. 2015). The 2015 El Niño-induced pattern (Fig. 21.2h) seems to be out of phase with the well-known PJ pattern (Wakabayashi and Kawamura 2004).

ENSO modifies the background state of tropical–subtropical ISO and thus significantly affects the degree of ISO modulation on TC formation in the WNP (Li et al. 2012). The El Niño in the summer 2015 provides the favorable background condition for the growth of tropical disturbances, including strengthened vorticity and monsoon trough within 5°–20°N (Fig. 21.2h). We examined a possible influence of El Niño on the intraseasonal PJ teleconnection pattern and associated SAT in Japan for July–August 2015 (Supplemental Fig. S21.4). The result indicates that the extreme rainfall accompanied by intraseasonal variability is more enhanced east of the Philippines, which may in turn cause more warming in Japan through the PJ teleconnection due to extreme El Niño in 2015 (see online Supplemental Material). This work notes that an understanding of the interaction between tropical SST and the intraseasonal teleconnection is of importance for weather and climate prediction for East Asia. A follow-up study using atmosphere–ocean coupled GCMs is required to investigate any role of air–sea interaction in extraordinary weather and climate in Japan.

Conclusions. The persistent Japanese heat wave that occurred in early August of 2015 was mainly attributed to intraseasonal disturbances, including TCs. Yet, it is found that the anthropogenic warming increased the probability of occurrence of the event by 1.5 to 1.7 times. The contribution of human-induced warming to the 2015 heat wave would have been more pronounced if there had not been a concurrent extreme El Niño event because El Niño has a cooling effect in Japan.

ACKNOWLEDGEMENTS. This work was supported by Grant-in-Aid 24241009 and the Program for Risk Information on Climate Change (SOUSEI program) from the Ministry of Education, Culture, Sports, Science and Technology (MEXT), Japan.

REFERENCES

Chen, G., and C. -H. Sui, 2010: Characteristics and origin of quasi-biweekly oscillation over the western North Pacific during boreal summer. *Geophys. Res. Lett.*, **115**, D14113, doi:10.1029/2009JD013389.

Christidis, N., and P. A. Stott, 2014: Change in the odds of warm years and seasons due to anthropogenic influence on the climate. *J. Climate*, **27**, 2607–2621, doi:10.1175/JCLI-D-13-00563.1.

Huffman, G. J., R. G. Adler, M. M. Morrissey, D. T. Bolvin, S. Curtis, R. Joyce, B. McGavock, and J. Susskind, 2001: Global precipitation at one-degree daily resolution from multi-satellite observations. *J. Hydrometeor.*, **2**, 36–50.

Imada, Y., H. Shiogama, M. Watanabe, M. Mori, M. Kimoto, and M. Ishii, 2014: The Contribution of anthropogenic forcing to the Japanese heat waves of 2013 [in "Explaining Extreme Events of 2013 from a Climate Perspective"]. *Bull. Amer. Meteor. Soc.*, **95 (9)**, S52–S54.

Kawamura, R., and T. Ogasawara, 2006: On the role of typhoons in generating PJ teleconnection Pattern over the western North Pacific in late summer. *SOLA*, **2**, 37–40, doi:10.2151/sola.2006-010.

Kobayashi, S., and Coauthors, 2015: The JRA-55 reanalysis: General specifications and basic characteristics. *J. Meteor. Soc. Japan*, **93**, 5–48, doi:10.2151/jmsj.2015-001.

Kubota, H., Y. Kosaka, and S.-P. Xie, 2015: A 117-year long index of the Pacific-Japan pattern with application to interdecadal variability. *Int. J. Climatol.*, **36**, 1575–1589, doi:10.1002/joc.4441.

Li, R. C., and W. Zhou, 2013: Modulation of western North Pacific tropical cyclone activity by the ISO. Part I: Genesis and intensity. *J. Climate*, **26**, 2904–2918, doi:10.1175/JCLI-D-12-00210.1.

——, W. Zhou, J. C. K. Chan, and P. Huang, 2012: Asymmetric modulation of western North Pacific cyclogenesis by the Madden–Julian oscillation under ENSO conditions. *J. Climate*, **25**, 5374–5385, doi:10.1175/JCLI-D-11-00337.1.

Madden, R. A., and P. R. Julian, 1971: Detection of a 40–50 day oscillation in the zonal wind in the tropical Pacific. *J. Atmos. Sci.*, **28**, 702–208.

Nitta, T., 1987: Convective activities in the tropical western Pacific and their impact on the Northern Hemisphere summer circulation. *J. Meteor. Soc. Japan*, **65**, 373–390.

Ogasawara, T., and R. Kawamura, 2007: Combined effects of teleconnection patterns on anomalous summer weather in Japan. *J. Meteor. Soc. Japan*, **85**, 11–24, doi:10.2151/jmsj.85.11.

Onogi, K., and Coauthors, 2007: The JRA-25 reanalysis. *J. Meteor. Soc. Japan*, **85**, 369–432, doi:10.2151/jmsj.85.369.

Rayner, N. A., Parker, E. B. Horton, C. K. Folland, L. V. Alexander, D. P. Rowell, E. C. Kent, and A. Kaplan, 2003: Global analyses of sea surface temperature, sea ice, and night marine air temperature since the late nineteenth century. *J. Geophys. Res.*, **108**, 4407, doi:10.1029/2002JD002670.

Shiogama, H., M. Watanabe, Y. Imada, M. Mori, M. Ishii, and M. Kimoto, 2013: An event attribution of the 2010 drought in the south Amazon region using the MIROC model. *Atmos. Sci. Lett.*, **14**, 170–175, doi:10.1002/asl2.435.

——, ——, ——, ——, Y. Kamae, M. Ishii, and M. Kimoto, 2014: Attribution of the June–July 2013 heat wave in the southwestern United States. *SOLA,* **10**, 122–126, doi:10.2151/sola.2014-025.

Simpson, I. R., T. A. Shaw, and R. Seager, 2014: A diagnosis of the seasonally and longitudinally varying midlatitude circulation response to global warming. *J. Atmos. Sci.*, **71**, 2489–2515, doi:10.1175/JAS-D-13-0325.1.

Stone, D., 2013: Boundary conditions for the C20C Detection and Attribution Project: The All-Hist/est1 and Nat-Hist/CMIP5-est1 scenarios. Lawrence Berkeley National Laboratory, 18 pp. [Available online at http://portal.nersc.gov/c20c/input_data/C20C-DandA_dSSTs_All-Hist-est1_Nat-Hist-CMIP5-est1.pdf.]

Wakabayashi, S., and R. Kawamura, 2004: Extraction of major teleconnection patterns possibly associated with the anomalous summer climate in Japan. *J. Meteor. Soc. Japan*, **82**, 1577–1588.

Watanabe, M., and Coauthors, 2010: Improved climate simulation by MIROC5: Mean states, variability, and climate sensitivity. *J. Climate*, **23**, 6312–6335, doi:10.1175/2010JCLI3679.1.

Yamada, K., and R. Kawamura, 2007: Dynamical link between typhoon activity and the PJ teleconnection pattern from early summer to autumn as revealed by the JRA-25 reanalysis. *SOLA*, **3**, 65–68, doi:10.2151/sola.2007-017.